Giant Rabi splitting between localized mixed plasmon-exciton states in a two-dimensional array of nanosize metallic disks in an organic semiconductor

J. Bellessa,[1,2] C. Symonds,[1,*] K. Vynck,[2] A. Lemaitre,[3] A. Brioude,[4] L. Beaur,[2] J. C. Plenet,[1] P. Viste,[1] D. Felbacq,[2] E. Cambril,[3] and P. Valvin[2]

[1]*Université de Lyon; Université Lyon 1, LPMCN; CNRS, UMR 5586, 69622 Villeurbanne, France*

[2]*GES, Université Montpellier II–CNRS, Case Courrier 074, F-34095 Montpellier Cedex 5, France*

[3]*LPN, CNRS, Route de Nozay, F-91460 Marcoussis, France*

[4]*Université de Lyon; Université Lyon 1, LMI; CNRS, UMR 5615, 69622 Villeurbanne, France*

(Received 4 June 2009; published 14 July 2009)

We study localized surface plasmons in strong coupling with excitons of organic semiconductors. The plasmons are localized in lithographed silver nanodisks organized in square array. A giant Rabi splitting energy of 450 meV is obtained, and typical behaviors of mixed states, i.e., anticrossing of their energies and crossing of their linewidths, are observed. Three-dimensional finite-difference time-domain simulations and coupled oscillator calculations are used to analyze and corroborate the experimental results.

DOI: 10.1103/PhysRevB.80.033303 PACS number(s): 78.66.Qn, 71.35.−y, 73.20.Mf, 78.67.Bf

Tailoring the optical properties of systems such as semiconductor microcavities and metal/semiconductor hybrid structures by acting on their environment is currently a subject of significant interest. Metallic nanoparticles are good candidates for this purpose due to the strong localization of the electromagnetic field within and in the proximity of the nanoparticle; luminescence[1,2] and Raman enhancement have been evidenced and applied to high-efficiency light-emitting diodes[3] and single particle Raman measurements,[4,5] respectively. When the emitters present high-oscillator strength, a strong coupling regime between plasmons and excitons can be reached, leading to the formation of mixed plasmon/exciton states. An anticrossing in the dispersion relations is then observed, the strength of the coupling being characterized by the Rabi splitting. This hybridization has been predicted theoretically for metallic nanoparticles interacting with an emitter,[6] where well-separated mixed states and a clear anticrossing have been observed. From an experimental point of view, the strong coupling regime has been demonstrated for delocalized plasmons on planar metal surfaces with a Rabi splitting energy of 300 meV,[7,8] on nanostructured metal surfaces,[9,10] and on close packed nanorods.[11] For localized surface plasmons (LSP) in metallic nanoparticles, luminescence enhancement has been observed in the weak coupling regime,[12] as well as coherent effects.[13] The formation of mixed LSP/exciton states with a Rabi splitting energy of 120 meV has been demonstrated recently in solutions of colloidal metallic nanoshells coupled to molecular exciton.[14] However the increase in the Rabi splitting energy compared to 2D plasmons, resulting from the localization of the plasmon, has never been observed.

In this work, the interaction between metallic nanodisks (NDs) organized in arrays by lithographic means and an organic semiconductor is studied. The main advantage of lithographed structures is that the size of the NDs and their environment (other disks and semiconductor) are well controlled, thereby avoiding a large inhomogeneous broadening of the plasmonic resonances, which could partially mask the plasmon/exciton hybridization. Furthermore, the lithography technique used is fully compatible with passive plasmonic devices, such as low-attenuation guides or plasmonic nanocavities developed recently. The obtained Rabi splitting energy is extremely large, 450 meV, arising from the combination of a large excitonic oscillator strength and a considerable enhancement of the electromagnetic field due to the LSPs. Systems where the Rabi splitting represents a significant part of the transition energy[15] are also of interest for the creation of correlated photon pair sources.[16]

The first part of this Brief Report deals with the ND fabrication and the characterization of the bare plasmon resonances. The Ag NDs have been defined by e-beam lithography on a glass substrate. A 60 nm thick silver film was evaporated and then removed by the lift-off technique, hence revealing the silver ND assemblies on the surface. Each assembly consists of a 200 by 200 μm array made of several tens of thousands of NDs separated by 210 nm side to side. Several arrays, with different ND diameters, were fabricated in order to tune the LSP resonance energy. The ND sizes range from 100 to 210 nm. Scanning electron microscope (SEM) images of the NDs were taken to determine the mean disk diameter and the ND size dispersion. A SEM image is shown in Fig. 1 as well as a typical size dispersion of NDs with a 140 nm mean diameter. The typical size dispersion is ± 7 nm and the distance between the NDs is 210 nm side to side. This distance has been chosen to cause a negligible interaction between the localized plasmons of neighboring NDs, in order to drastically limit the influence of the environment on the coupling between the plasmon of a single

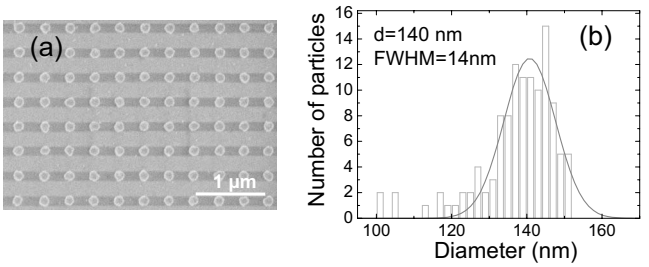

FIG. 1. (a) SEM image of a NDs array. (b) Typical size distribution of the ND diameters.

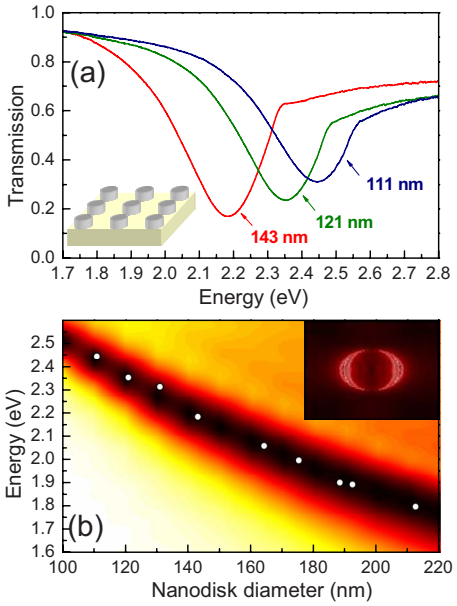

FIG. 2. (Color online) (a) Transmission spectra of the bare NDs for 111, 121, and 143 nm diameters. (b) Measured energy positions of the LSPs resonances (white circles) as a function of the ND diameter, superimposed on the transmission spectra obtained from 3D FDTD calculations (in color/grayscale). The inset presents the calculated norm of the LSP electric field for a 140 nm ND.

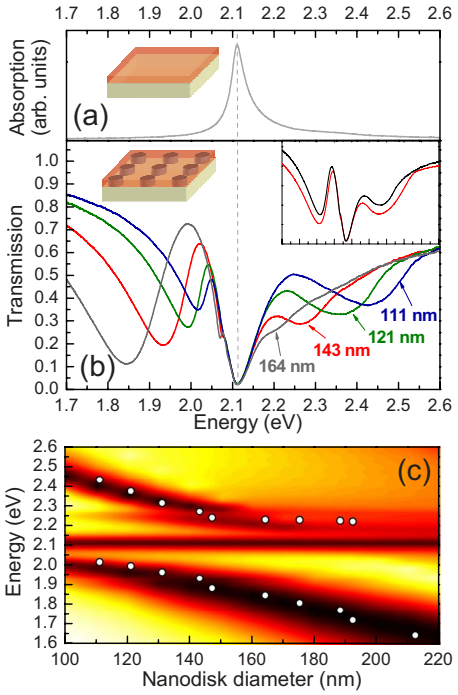

FIG. 3. (Color online) (a) TDBC absorption measured in a region without NDs. (b) Transmission spectra of the TDBC-covered samples for different ND diameters (111, 121, 143, and 164 nm). The inset shows transmission spectra of two arrays with the same ND diameter (132 nm), and interdisk distances of 190 nm (red/gray line) and 210 nm (black line) with the same energy scale than the main figure. (c) Measured energies of the transmission dips (white circles) as a function of the ND diameter, superimposed on the transmission spectra obtained from 3D FDTD calculations (in color/grayscale).

disk and semiconductor excitons. Indeed, the interdisk coupling becomes negligible when the disk diameter is smaller than the separation distance.[17] The influence of the array on the coupling effect described in the following is therefore negligible. Diffractive effects can also be observed in periodic nanoparticle arrays, which can result in variations in the plasmon dip depth without significant energy modification[18] or in the emergence of sharp peaks in the optical spectra.[19] However, to observe such peaks the nanoparticles have to be imbedded in a homogeneous medium, as shown by Auguie *et al.*,[19] which is not the case in our experiments where the nanodisks are surrounded by glass on one side and air or dye on the other sides.

All the transmission experiments were done at room temperature on circular regions of 50 μm diameter (probing around 2×10^4 identical NDs). Figure 2(a) shows the transmission spectra recorded for three arrays having three different ND diameters. A pronounced dip is observed for each array, associated to the ND LSP resonance. The plasmon resonance energy, measured from the transmission minimum, is plotted in Fig. 2(b) as a function of the disk diameter. It shifts from 1.8 to 2.45 eV while its width remains quasiconstant, about 180 meV. This linewidth includes both a homogeneous and an inhomogeneous broadenings. The latter mainly arises from the Gaussian ND size distribution and can be deduced from the dispersion measured from the SEM images (±7 nm) and the size/energy relation extracted from Fig. 2(b). This inhomogeneous broadening is estimated to 90 meV. Supposing that the total width is the quadratic addition of the homogeneous and inhomogeneous widths (convolution of two Gaussian lines), the homogeneous broadening is estimated to 155 meV. Transmission spectra were simulated with three-dimensional (3D) finite-difference time-domain (FDTD) calculations using a freely available software package.[20] The silver dielectric constant was fitted to the values reported by Johnson *et al.*[21] using a Drude model with an instantaneous dielectric function of 3.70, a plasma frequency of 13740×10^{12} rad.s^{-1} and a damping coefficient of 32.1×10^{12} rad.s^{-1}. The calculated transmission spectra are shown on color map as a function of the ND diameter in Fig. 2(b). An excellent agreement with the experimental data is obtained. The calculated norm of the LSP electric field for a 140 nm diameter ND is presented in the Fig. 2(b) inset, showing an intense confinement of the electric field around the particle.

We now turn to the coupled exciton/plasmon system. The active layer is a thin film of a cyanine dye *J*-aggregate [5,5′, 6,6′-tetrachloro-1,1′-diethyl-3,3′-di(4-sulfobutyl)-benzimidazolo-carbocyanine, or TDBC] diluted in water and spin coated onto the whole sample surface. The TDBC monomers form linear chains, namely, *J*-aggregates. This ordering of the dye molecules creates a delocalization of the excitation which induces a redshift and a narrowing of the absorption band.[22] Figure 3(a) presents the absorption spectrum of a TDBC layer deposited onto a blank glass substrate. The pronounced maximum lying at about 2.11 eV, with a linewidth of 52 meV, corresponds to the *J*-band absorption.

In a first series of experiments, the ND assemblies were

coated with a TDBC layer. Typical transmission spectra are presented for four ND diameters in Fig. 3(b). Three well-defined dips clearly appear in each spectrum. It should be noted that, in the case of a weak interaction between the plasmon and the *J*-aggregate exciton, only two dips would be present, assigned to the dye absorption and the plasmon mode. The presence of three dips is therefore a strong indication of the plasmon/exciton hybridization, which leads to the formation of two distinct mixed states at energies differing from those of the bare plasmon and exciton. The center peak is clearly related to the bare, uncoupled exciton, its energy position (2.11 eV) corresponding to the *J*-aggregate absorption maximum [Fig. 3(a)]. This peak is expected since the NDs occupy only about 10% of the sample surface, leaving a significant part of dye noninteracting with the LSP. The energy positions of the two dips present on both energy sides of the dye absorption have been reported as a function of the ND diameter in Fig. 3(c). The two lines experience a blue shift as the ND diameter is increased, as well as a clear anticrossing, characteristic of the strong coupling regime between the plasmon and the exciton. These two transitions correspond to the upper and lower-energy plasmon/exciton mixed states (UMS and LMS, respectively). The resonance, which occurs when separation in energy between both transitions is the smallest, is achieved for NDs with a diameter around 143 nm. This energy separation, called Rabi splitting energy, is very large (337 meV). In order to confirm these results, transmission spectra have been calculated with the 3D FDTD method. The dispersion of the dye has been modeled by a Lorentzian with an instantaneous dielectric constant of 2.56 and a Lorentz oscillator of frequency 3206×10^{12} rad.s^{-1}, spectral width 48.6×10^{12} rad.s^{-1} and strength 0.4155. Based on a series of 3D FDTD calculations, we have considered that a dye layer of thickness 12.5 nm has been deposited onto the sample. The calculated spectra, displayed in color map in Fig. 3(c), are in very good agreement with the measurements, reproducing with an excellent accuracy the anticrossing that is observed experimentally. The inset of Fig. 3(b) presents the transmission spectra of two arrays with the same ND diameter (132 nm) but different interdisk distances (190 and 210 nm). The spectra have a similar shape with the same dip energy positions giving a confirmation that the distance between the disks does not influence the plasmon exciton coupling, and that the important parameter is the disk diameter.

Another confirmation of the occurrence of the plasmon-exciton mixing can be found when analyzing both UMS and LMS transition linewidths. They are plotted in Fig. 4(b), together with the bare plasmon and bare exciton absorption linewidths (180 and 52 meV respectively) deduced from the absorption spectra. As the ND diameter is increased, an inversion in the mixed state linewidths occurs. This feature is characteristic of the strong coupling regime, resulting from the hybrid nature of the mixed states. It can be understood considering a coupled oscillator model, with the following plasmon-exciton Hamiltonian:

$$H = \begin{pmatrix} E_{\mathrm{pl}}(d) - i\gamma_{\mathrm{pl}} & \Delta/2 \\ \Delta/2 & E_{\mathrm{ex}}(d) - i\gamma_{\mathrm{ex}} \end{pmatrix},$$

where d is the ND diameter, Δ the interaction energy (360 meV), E_{ex} the uncoupled exciton energy (2.11 eV), γ_{ex} the exciton linewidth (52 meV). E_{pl}(d) is the bare plasmon energy, deduced from 3D FDTD calculations, and γ_{pl} the plasmon homogeneous broadening (155 meV) extracted using the procedure described above. The mixed state widths have been calculated using the homogeneous linewidths of the plasmon and the exciton, considering that the NDs are quasi-isolated from their neighbors and are not sensitive to the size dispersion. The inhomogeneous broadening appears because several thousands of NDs were experimentally probed at the

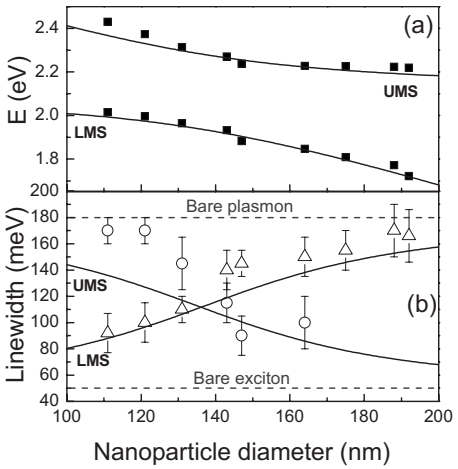

FIG. 4. (a) Measured (squares) and calculated (solid lines) mixed states energy positions as a function of the ND diameter. (b) Measured (open circles and triangles) and calculated (solid lines) mixed states linewidths. The dashed lines correspond to the bare plasmon and exciton linewidths.

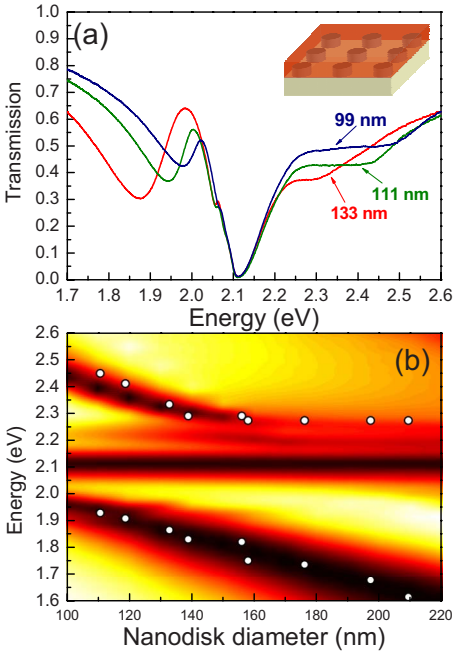

FIG. 5. (Color online) (a) Transmission spectra of the samples covered with two TDBC layers recorded for three different ND diameters (99, 111, and 133 nm). (b) Measured energies of the transmission dips (white circles) as a function of the ND diameter, superimposed on the transmission spectra obtained from 3D FDTD calculations (in color/grayscale).

same time and is quadratically added to the homogeneous width obtained from the coupled oscillator model. As can be seen in Fig. 4(a), this simple model reproduces well the experimental mixed state energies. The crossing of the mixed state linewidths occurs at the resonance (calculated diameter 136 nm), in agreement with the experimental data [Fig. 4(b)], and consistent with an equal-weight mixing between the plasmon and the exciton for this ND diameter.

In a second series of experiments, in order to check the influence of the exciton absorption on the coupling strength, an additional TDBC layer has been spin coated onto the previous one. The transmission spectra recorded for 99, 111, and 133 nm diameter NDs are presented in Fig. 5(a). The mixed state energies are presented as a function of the ND diameter in Fig. 5(b), together with the normalized transmission obtained from 3D FDTD calculations in which a dye layer of total thickness 22.5 nm has been considered. The main difference with the previous series of experiments is the larger energy splitting between the two dispersion curves. This behavior is consistent with the increase in the dye layer absorption.[8] The calculated and the experimental values are again in excellent agreement. The Rabi splitting amounts to 450 meV, which is the highest value reported up to now. It should be noted that the UMS dips in Fig. 5(a) are less pronounced than those in Fig. 3(b). This comes from the high-energy tail of the TDBC absorption, which does not modify the mixed state energy but reduces the dip depth in the transmission spectra. This effect was already observed by Bonnand *et al.*[8] This behavior becomes readily apparent as the aggregated dye layer thickness is increased.

To conclude, we have shown that mixed states can be obtained for metallic NDs interacting with an organic semiconductor. The Rabi splitting energy obtained is very large (450 meV, 20% of the transition energy). These systems may serve as model for a large variety of filled nanoparticles, e.g., spheres or ellipsoids, with well-controlled conditions of environment and particle size. Furthermore, the compatibility of our system with passive plasmonic devices opens the way to the realization of complex architectures where the plasmon properties will be tailored not only by the metal nanostructuration, but also by hybridization with an active material.

This work has been supported by the project SCOP from the french Agence Nationale de la Recherche.

*clementine.symonds@lpmcn.univ-lyon1.fr

[1] O. Kulakovich, N. Strekal, A. Yaroshevich, S. Maskevich, S. Gaponenko, I. Nabiev, U. Woggon, and M. Artemyev, Nano Lett. **2**, 1449 (2002).
[2] P. Anger, P. Bharadwaj, and L. Novotny, Phys. Rev. Lett. **96**, 113002 (2006).
[3] M. K. Kwon, J. Y. Kim, B. H. Kim, I. K. Park, C. Y. Cho, C. C. Byeon, and S. J. Park, Adv. Mater. **20**, 1253 (2008).
[4] Surface Enhanced Raman Scattering, in edited by R. K. Chang and T. E. Furtak (Plenum Press, New York, 1982).
[5] N. Félidj, J. Aubard, G. Lévi, J. R. Krenn, M. Salerno, G. Schider, B. Lamprecht, A. Leitner, and F. R. Aussenegg, Phys. Rev. B **65**, 075419 (2002).
[6] T. Ambjörnsson, G. Mukhopadhyay, S. P. Apell, and M. Käll, Phys. Rev. B **73**, 085412 (2006).
[7] J. Bellessa, C. Bonnand, J. C. Plenet, and J. Mugnier, Phys. Rev. Lett. **93**, 036404 (2004).
[8] C. Bonnand, J. Bellessa, and J. C. Plenet, Phys. Rev. B **73**, 245330 (2006).
[9] Y. Sugawara, T. A. Kelf, J. J. Baumberg, M. E. Abdelsalam, and P. N. Bartlett, Phys. Rev. Lett. **97**, 266808 (2006).
[10] J. Dintinger, S. Klein, F. Bustos, W. L. Barnes, and T. W. Ebbesen, Phys. Rev. B **71**, 035424 (2005).
[11] G. A. Wurtz, P. R. Evans, W. Hendren, R. Atkinson, W. Dickson, R. J. Pollard, and A. V. Zayats, Nano Lett. **7**, 1297 (2007).
[12] J. S. Biteen, N. S. Lewis, H. A. Atwater, H. Mertens, and A. Polman, Appl. Phys. Lett. **88**, 131109 (2006).
[13] G. P. Wiederrecht, G. A. Wurtz, and J. Hranisavljevic, Nano Lett. **4**, 2121 (2004).
[14] N. T. Fofang, T. H. Park, O. Neumann, N. A. Mirin, P. Nordlander, and N. J. Halas, Nano Lett. **8**, 3481 (2008).
[15] E. Dupont, J. A. Gupta, and H. C. Liu, Phys. Rev. B **75**, 205325 (2007).
[16] C. Ciuti, G. Bastard, and I. Carusotto, Phys. Rev. B **72**, 115303 (2005).
[17] L. Gunnarsson, T. Rindzevicius, J. Prikulis, B. Kasemo, M. KallShengli, S. Zou, and G. C. Schatz, J. Phys. Chem. B **109**, 1079 (2005).
[18] A. Hohenau, J. R. Krenn, J. Beermann, S. I. Bozhevolnyi, S. G. Rodrigo, L. Martin-Moreno, and F. Garcia-Vidal, Phys. Rev. B **73**, 155404 (2006).
[19] B. Auguie and W. L. Barnes, Phys. Rev. Lett. **101**, 143902 (2008).
[20] MIT Electromagnetic Equation Propagation (MEEP).
[21] P. B. Johnson and R. W. Christy, Phys. Rev. B **6**, 4370 (1972).
[22] *J-Aggregates*, edited by T. Kobayashi (World Scientific, Singapore, 1996).